Geophysical Research Letters

RESEARCH LETTER
10.1029/2018GL080563

Temperature- and Humidity-Dependent Phase States of Secondary Organic Aerosols

Sarah S. Petters[1,2], Sonia M. Kreidenweis[1], Andrew P. Grieshop[3], Paul J. Ziemann[4], and Markus D. Petters[5]

[1]Department of Atmospheric Science, Colorado State University, Fort Collins, CO, USA, [2]Now at the Department of Environmental Sciences and Engineering, University of North Carolina at Chapel Hill, Chapel Hill, NC, USA, [3]Department of Civil, Construction and Environmental Engineering, North Carolina State University, Raleigh, NC, USA, [4]Department of Chemistry and Cooperative Institute for Research in Environmental Sciences (CIRES), University of Colorado at Boulder, Boulder, CO, USA, [5]Department of Marine, Earth, and Atmospheric Sciences, North Carolina State University, Raleigh, NC, USA

Key Points:
- Differences in composition and hygroscopicity shift humidified viscosity isopleths for secondary organic aerosols at cold temperatures
- Temperature dependence of viscosity for dry secondary organic aerosol was similar to that of citric acid, coal tar pitch, and sorbitol
- For monoterpene-derived secondary organic aerosols, the temperature where viscosity was 10^6 Pa·s was anticorrelated with oxidation state

Supporting Information:
- Supporting Information S1

Correspondence to:
S. S. Petters,
spetters@unc.edu

Citation:
Petters, S. S., Kreidenweis, S. M., Grieshop, A. P., Ziemann, P. J., & Petters, M. D. (2019). Temperature- and humidity-dependent phase states of secondary organic aerosols. *Geophysical Research Letters*, *46*, 1005–1013. https://doi.org/10.1029/2018GL080563

Received 24 SEP 2018
Accepted 22 DEC 2018
Accepted article online 28 DEC 2018
Published online 16 JAN 2019

Abstract Viscosity of monoterpene-derived secondary organic aerosols (SOAs) as a function of temperature and relative humidity (RH), and dry SOA glass transition temperatures are reported. Viscosity was measured using coalescence time scales of synthesized 100 nm dimers. Dry temperature-dependent SOA viscosity was similar to that of citric acid, coal tar pitch, and sorbitol. The temperature where dry viscosity was 10^6 Pa·s varied between 14 and 36 °C and extrapolated glass transition varied between −10 and 20 °C (±10 °C). Mass fragment f_{44} obtained with an Aerosol Chemical Speciation Monitor was anticorrelated with viscosity. Viscosity of humidified Δ^3-carene and α-pinene SOAs exceeded 10^6 Pa·s for all subsaturated RHs at temperatures <0 and −5 °C, respectively. Steep viscosity isopleths at 10^6 Pa·s were traced for these across (temperature, RH) conditions ranging from (approximately −5 °C, 100%) and (approximately 36 °C, 0%). Differences in composition and thus hygroscopicity can shift humidified viscosity isopleths for SOAs at cold tropospheric temperatures.

Plain Language Summary Airborne particles in the environment can be harmful to human health and are part of the climate system. These particles and any harmful substances they may carry can be broken down by oxidants or removed by water. This is easier if the particles are liquid and becomes more difficult if particles are semisolid (like peanut butter) or solid (like glass). However, viscosity is hard to measure for nanoscale airborne particles. Recent advances have made this possible. In this study we measured the viscosity of several types of oxidized organic aerosols at different temperatures and humidities. We collided and melted together 100 nm particles in a continuous flow system. Without moisture, the particles were as hard as pitch and melted between 14 and 36 °C. At temperatures 20° colder they could be considered as hard as glass. The chemical marker for more oxidized material was correlated with softer particles. Below −5° we were unable to liquefy the particles even with high relative humidity. The particles melted at about −5° at 100% relative humidity and at 36° dry, with intermediate points connecting these extremes. We found that the composition and water solubility of the particles affects their viscosity at cold temperatures.

1. Introduction

Several laboratory studies have reported that secondary organic aerosols (SOAs) can exist in viscous semi-solid or glassy states at low relative humidity (RH). These include SOA formed from oxidation of isoprene (Song et al., 2015), monoterpene (Grayson et al., 2016; Järvinen et al., 2016; Pajunoja et al., 2014; Renbaum-Wolff et al., 2013; Zhang et al., 2015), and aromatic (Saukko et al., 2012; Song et al., 2016) precursors. High viscosity is associated with slower diffusion (Zobrist et al., 2008), intraparticle mixing (Ye et al., 2016), and multiphase chemistry (Gržinić et al., 2015; Slade & Knopf, 2014) and can trap carcinogens inside the organic matrix (Shrivastava et al., 2017; Zelenyuk et al., 2012). Taking RH dependence into account, Shiraiwa et al. (2017) estimate that SOA is semisolid to glassy in the boundary layer over midlatitude dry areas (United States, most of Europe) and liquid over the tropics and arctic, where RH is higher. Most experimental studies investigate SOA at room temperature and report viscosity decreasing with increasing RH. To our knowledge, the temperature-dependent SOA viscosity and glass transition temperatures (T_g) of dry SOAs have not been reported (Reid et al., 2018). Complete

amorphous phase diagrams quantifying aerosol viscosity as a function of temperature (T) and RH are necessary for accurate prediction of SOA phase in next generation models that predict SOA composition, size distributions, and mass (Zaveri et al., 2014).

Here we present experimentally derived phase diagrams for SOAs undergoing induced viscosity transitions at 10^6 Pa·s. SOA was generated by oxidizing monoterpenes inside a laminar flow tube reactor. Variable T and RH were used to induce a viscous transition of particle dimers into spheres using an aerosol coalescence and isolation technique (Marsh et al., 2018; Rothfuss & Petters, 2016, 2017a). Dry experiments probed the T-dependent viscosity transition at 10^6 Pa·s and T_g was determined by extrapolating to the glass transition viscosity. Dry viscosities were compared to chemical composition using an Aerosol Chemical Speciation Monitor (ACSM).

2. Materials and Methods

2.1. SOA Generation

SOA precursors included α-pinene (Aldrich, 99%), Δ^3-carene (Aldrich, >90%), myrcene (Aldrich, >95%), limonene (Aldrich, 99%), and ocimene (Aldrich, >90%), all used without further purification. SOA was generated in a laminar stainless steel continuous-flow tube reactor similar in inlet design and dimensions to that of Bilde et al. (2003). A zero-air generator (Teledyne 701) supplied the reactor with hydrocarbon-free air. Sheath and central flows were introduced by separate inlets and the central inlet included a variable-depth injector. The sheath:central flow ratio was 1.2:0.4 L/min and the average residence time in the flow reactor was 65 s. Ozone was generated at high concentration (~2,000 ppm) via corona discharge and injected into the central flow. Liquid monoterpene was injected and evaporated at 35 nl/min into the sheath flow. The high O_3 concentrations were used to oxidize the precursor on short time scales. After the reactor, most O_3 was removed by passing the aerosol through a diffusion dryer filled with catalyst (Carulite 200 Mesh) to quench further chemical reaction and to protect the equipment. Ozone concentrations were measured using UV absorption at 254 nm (2B technologies) after the catalyst and ranged from 0.5 to 3 ppmv. The aerosol was then routed to either a viscosity measurement, a Scanning Mobility Particle Sizer (SMPS; described by S. S. Petters & Petters, 2016) or an ACSM (Ng et al., 2011). The size distribution of the SOA stabilized after ~2 hr with a mode diameter ~100 nm and SMPS-derived volume concentrations ranging between 1,950 and 3,500 $\mu m^3/m^3$. The ACSM (inlet flow 0.1 L/min) sampled particles downstream of the SMPS, set to select 100 nm particles, and a variable dilution flow to avoid saturating the detector. Mass concentrations in the ACSM ranged between 10 and 40 $\mu g/m^3$ and mass spectra were recorded for ~10 min for each SOA. The ACSM mass spectra were used to find the fraction of SOA mass at $m/z = 44$ (f_{44}) and $m/z = 43$ (f_{43}).

2.2. Viscosity Measurements

Viscosity near 10^6 Pa·s was measured as a function of T and RH by inducing a viscous transition between 4×10^5 and 6×10^6 Pa·s, centered near 10^6 Pa·s. Due to the methods employed, throughout this work we discuss viscosity in terms of the thermodynamic conditions under which viscosity change was observed. Extrapolated dry viscosities at $0 \leq T \leq 30$ °C are given in the supporting information (SI).

The setup has been described previously (see Marsh et al., 2018, Figure 1). Two differential mobility analyzers (sheath:sample flow 3:0.5 L/min) of opposite polarity were used to select 100 nm particles carrying opposite charge. The aerosol streams were combined and particles coagulated in a chamber to form charge-neutral dimers. Charged particles were removed using an electrostatic filter. Neutral dimers were passed through a temperature-controlled conditioner with a residence time of 5 s. In the conditioner, either T or RH was varied to induce partial or complete relaxation from hourglass shapes into spheres. The mobility diameter of the dimers was scanned downstream using an SMPS (sheath:sample flow 1:0.3 L/min). The peak mobility diameter contains information about particle shape, and the dimer coalescence technique allows viscosity to be calculated from changing shape. Viscosity was calculated from monomer diameter (100 nm), coalescence time scale (5 s), and surface tension (0.03 N/m) using the algorithm of Rothfuss and Petters (2016). Calculations are described elsewhere (Marsh et al., 2018; Rothfuss & Petters, 2016) and in the SI. Surface tension was assumed based on typical values for pure organic liquids (Korosi & Kovats, 1981) and α-pinene-derived SOA (Hritz et al., 2016). For 100 nm monomers the viscosity transition measurement is near 10^6 Pa·s.

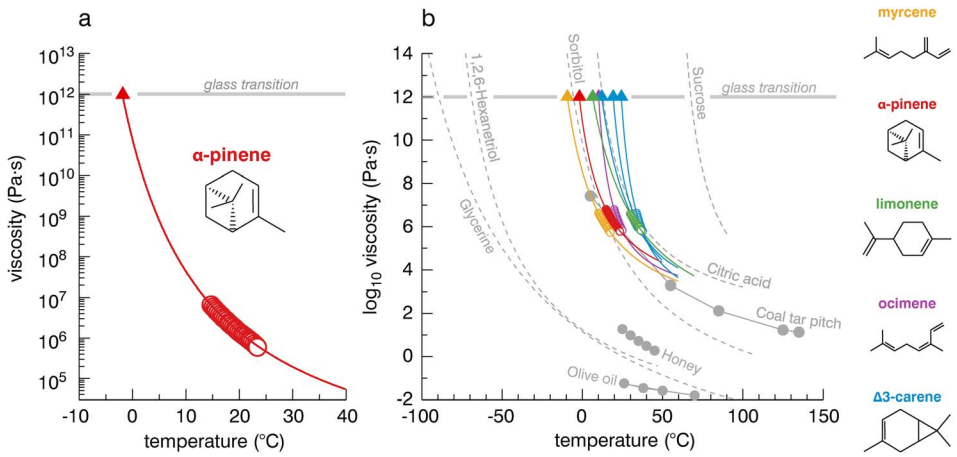

Figure 1. Temperature-dependent viscosities and extrapolation to T_g of dry SOAs. Colored circles show viscosity derived from the fit of the transition from uncoalesced to coalesced (Figure S1); lines show Vogel-Fulcher-Tammann fits to the viscosity; and triangles show T_g. Gray filled circles and dashed lines are data/Vogel-Fulcher-Tammann fits from the literature (tabulated in the supporting information). (a) α-pinene-derived SOA; (b) five SOAs, including three measurements for Δ^3-carene-derived SOA, compared to other substances (Diamante & Lan, 2014; Wood & Downer, 1965; Yanniotis et al., 2006). Colors match side illustrations showing precursor structures. SOA = secondary organic aerosol.

The coagulation chamber, electrostatic filter, conditioner, and SMPS were placed in an insulated box whose temperature was held constant at various setpoints between −22 and 30 °C using a recirculating chiller (hereafter referred to as *system T*). Accurate operation of the SMPS down to −22 °C has been demonstrated (Wright et al., 2016). Conditioner T or RH was varied using either isothermal humidification (RH-scans) or dry (RH ≤0.5%) temperature scans (T-scans). To prevent dimer relaxation outside the 5 s conditioner residence time, the system T was held at least 5 °C colder (for T-scans) or 5 °C warmer (for RH-scans) than the conditioner. Temperatures were measured by thermistors with ±1.0 °C accuracy. Humidification was achieved by passing zero-air through a Nafion humidifier at 0.1–1 L/min and flowing this into the coagulation chamber. Humidity was measured using a chilled mirror hygrometer with ±0.2 °C dewpoint/frostpoint accuracy, and was varied by changing the humidifier T and flow rate. System T, conditioner T, conditioner RH, and associated uncertainties for each experiment are reported in the SI.

2.3. Glass Transition Temperatures

Glass transition temperatures were calculated for dry SOAs by extrapolating the T-dependent viscosity to the glass transition point using a fit to the Vogel-Fulcher-Tammann (VFT) equation (Fulcher, 1925): $\log_{10}\eta = A + B/(T - T_0)$. Here η is viscosity and A, B, and T_0 are fitted constants. Dry experiments were performed for all SOAs to determine both T at the midpoint of dimer relaxation (~10^6 Pa·s) and the values of A, B, and T_0. Based on the convention that glass transition occurs at 10^{12} Pa·s (Debenedetti & Stillinger, 2001), the VFT equation yields $T_g = B/(12 - A) + T_0$.

3. Results and Discussion

Figure 1 shows the temperature dependence of viscosity for five SOAs in the context of a range of substances. Data from the T-scans, VFT fit parameters, and extrapolated T_g and viscosities in the range $0 \le T \le 30$ °C are tabulated in the SI. The temperature of the 10^6 Pa·s transition varied between 14 and 36 °C for these dry SOAs and was not correlated with precursor structure. The uncertainty in this temperature is <2 °C based on the 95% confidence interval of the fit (Table S1). Uncertainty in estimated viscosity due to the assumed surface tension is negligible (Marsh et al., 2018). Estimated values for T_g are 12–27 °C below the T associated with the 10^6 Pa·s transition. The uncertainty of the extrapolated T_g is ±10 °C based on validation with sucrose, citric acid, and binary mixtures of sucrose/citric acid and sucrose/sodium nitrate (Marsh et al., 2018; Rothfuss & Petters, 2017a). Viscosity of dry SOAs covers a relatively narrow range and is similar to that of citric acid, coal tar pitch, and sorbitol.

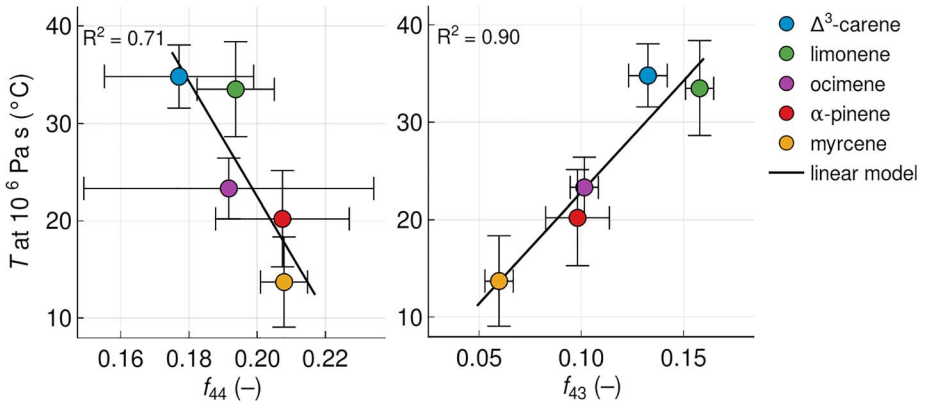

Figure 2. Temperature of the 10^6 Pa·s viscosity as a function of f_{44} and f_{43} measured by the Aerosol Chemical Speciation Monitor. Vertical bars correspond to the viscosity transition from 4×10^5 to 6×10^6 Pa·s, defined by the standard deviation of the logistic curve (Figure S1). Horizontal bars correspond to one standard deviation of the data. Coefficients of determination (R^2) for the linear models are shown in the top left corners.

Comparison with literature values is possible for a subset of our measurements. The viscosity of terpene-derived SOAs has been studied by various investigators using a wide range of techniques (Abramson et al., 2013; Bateman et al., 2015; Grayson et al., 2016; Hinks et al., 2016; Hosny et al., 2016; Järvinen et al., 2016; Kidd et al., 2014; Pajunoja et al., 2014, 2015; Price et al., 2015; Renbaum-Wolff et al., 2013; Saukko et al., 2012; Yli-Juuti et al., 2017; Zhang et al., 2015). Most of these studies focused on α-pinene, the majority of which have shown that viscosity of dry α-pinene-derived SOA is $\geq 10^6$ Pa·s at room temperature (Abramson et al., 2013; Grayson et al., 2016; Pajunoja et al., 2014; Renbaum-Wolff et al., 2013; Yli-Juuti et al., 2017; Zhang et al., 2015). This is consistent with our result (1.5×10^6 Pa·s at 20 °C; see Table S2). However, α-pinene-derived SOA viscosities vary greatly between studies, and this is discussed below. The diversity of results is also apparent with ice nucleation measurements for SOA at cirrus temperatures (Charnawskas et al., 2017; Ignatius et al., 2016; Wagner et al., 2017), which is thought to be controlled in part by viscosity (e.g., Baustian et al., 2013; Berkemeier et al., 2014; Murray et al., 2010). The wide range of results for SOA from one precursor complicates comparisons between precursors. For example, Hosny et al. (2016) show that myrcene-derived SOA viscosities overlap α-pinene-derived SOA viscosities from their own work and from Price et al. (2015) but are less viscous than α-pinene-derived SOA of Renbaum-Wolff et al. (2013). In this work, myrcene-derived SOA viscosity is lower than that of α-pinene at room temperature (3.3×10^5 vs 1.5×10^6 Pa·s). Hinks et al. (2016) show that limonene-derived SOA is less viscous than α-pinene-derived SOA, in contrast with our observations but at much lower mass loading. Elucidation of relationships between SOA types and viscosity is not possible without better understanding of compositional differences and how these relate to reaction conditions. In the coming years, collaborative viscosity intercomparison experiments and viscosity models for laboratory conditions could provide clarification.

Figure 2 shows that the measured temperature of the 10^6 Pa·s transition is inversely correlated with f_{44} and positively correlated with f_{43}. Similar correlations are observed for the extrapolated T_g (Figure S2). The fragments f_{44} and f_{43} are proxies for the elemental O:C and H:C ratios of the SOA mixture, respectively (Aiken et al., 2008). Oxidation state can be obtained as O:C − 2 × H:C (Kroll et al., 2011). The trend therefore implies that increasing oxidation state decreased viscosity. The following paragraph discusses this trend.

Organic viscosity is sensitive to a number of factors. Viscosity increases with the number of functional groups attached to the carbon chain, compound molecular weight, and depends on molecular structure (Koop et al., 2011; Rothfuss & Petters, 2017b). Parameterizations of T_g based on single component data include appropriate terms for O:C ratio and molecular weight (Shiraiwa et al., 2017). The inverse relationship with O:C (e.g., with f_{44}) in Figure 2 implies covarying molecular weight. The measured f_{44} fractions suggest that these SOAs are highly oxidized (e.g., Lambe et al., 2011). Therefore, it is plausible that differences in molecular size explain the observed trend between SOA from different precursors. This is consistent with measurements by Collier and Brooks (2016), who show that oxidation of squalene, which undergoes functionalization, increased its viscosity, whereas oxidation of squalane decreased its viscosity due to

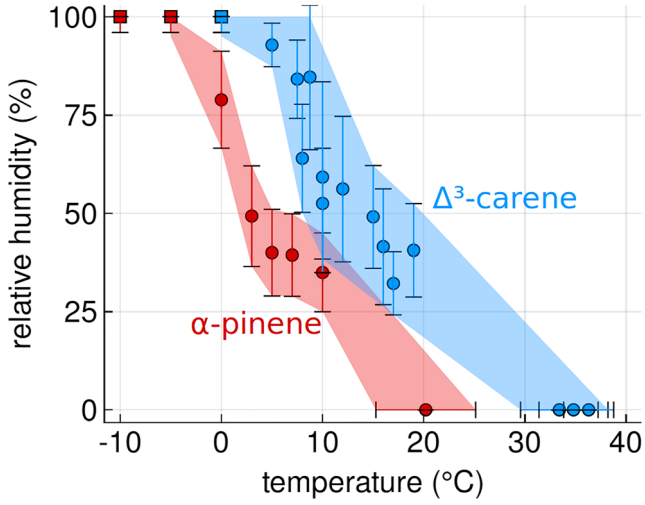

Figure 3. Viscous phase transitions of secondary organic aerosol derived from oxidation of Δ^3-carene and α-pinene, as a function of *T* and RH. Circles correspond to the midpoint of one *T* or RH scan and correspond to 10^6 Pa·s. Points at 0% RH show *T*-scans. Horizontal bars (*T* scans) and vertical bars (RH-scans) show the viscosity transition from 4×10^5 to 6×10^6 Pa·s, defined by the standard deviation of the logistic curve (Figure S1). Shaded areas circumscribe the transition regime (for coordinates see supporting information). Squares show experiments where viscosity did not change at the highest measured RH (96–100%). RH = relative humidity.

molecule fragmentation. A quick survey of sensitivity to known factors controlling viscosity reveals that the ~30 °C differences in observed viscosity transition shown in Figure 2 could be explained by the difference of a single polar functional group such as hydroxyl (OH) or carboxyl (O=COH; Rothfuss & Petters, 2017b); structural differences in organic molecules of otherwise identical composition (Rothfuss & Petters, 2017b); a difference in molecular weight of ~30 Da (~1 °C/Da; Shiraiwa et al., 2017); or a combination of these effects.

Figure 3 summarizes the *T*- and RH-dependent experiments showing the transition from 4×10^5 to 6×10^6 Pa·s. The graph can be interpreted as an amorphous phase state diagram. Conditions colder than the shaded area correspond to more viscous states, rapidly approaching glassy states ~20 to 30 °C below the observed transition (Figure 1 and Marsh et al., 2018; Rothfuss & Petters, 2017a). Conditions warmer than the shaded area correspond to less viscous states. The transition regions for Δ^3-carene-derived SOA and α-pinene-derived SOA are offset by 10 to 15 °C. Furthermore, the transition region appears to be wider for the Δ^3-carene-derived SOA than for the α-pinene-derived SOA. This could be because more repeat experiments were performed for Δ^3-carene, but the difference is also noticeable for individual scans. Colder than 0 °C (Δ^3-carene) or −5 °C (α-pinene), relaxation into a sphere was not observed at any subsaturated RH (RH < 96%).

Figure 4 shows the α-pinene-derived SOA transition between 4×10^5 and 6×10^6 Pa·s in the context of published studies. Here sucrose and citric acid are included as representative viscous organic aerosols and because their amorphous phase transitions are well understood based on multiple studies. Sucrose data (Rothfuss & Petters, 2017a) and sucrose and citric acid models (Marsh et al., 2018; Rothfuss & Petters, 2017a) correspond to a viscosity of 5×10^6 Pa·s. Citric acid data are omitted to avoid clutter. Several published α-pinene-derived SOAs are shown. Data from Järvinen et al. (2016) correspond to a viscosity of ~10^7 Pa·s. Data from Zhang et al. (2015) and Grayson et al. (2016) were included by finding the reported RH at 10^6 Pa·s. Although viscosities are slightly mismatched between data sets in Figure 4, the viscosities overlap at the edges of the respective measurement ranges and are close enough to permit evaluation of trends. Note that additional α-pinene-derived SOA observations (Abramson et al., 2013; Bateman et al., 2015; Hinks et al., 2016; Kidd et al., 2014; Pajunoja et al., 2014, 2015; Renbaum-Wolff et al., 2013; Saukko et al., 2012) were omitted because thermodynamic conditions where viscosity is near 10^6 Pa·s could not be derived from the reported data.

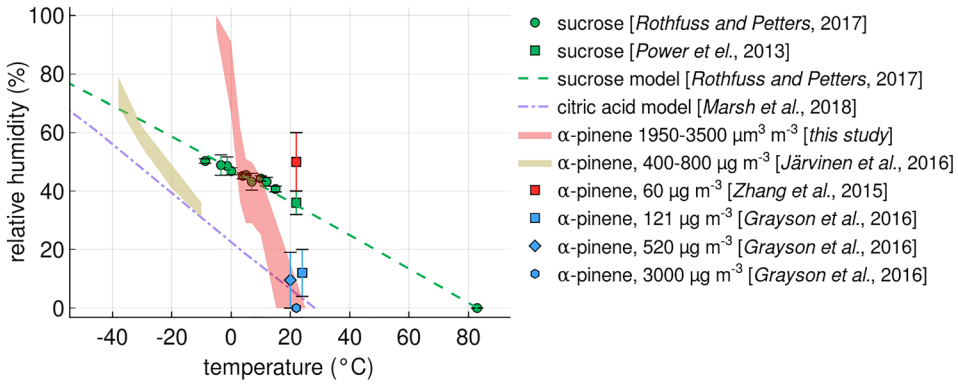

Figure 4. Comparison of α-pinene-derived secondary organic aerosol data with published studies. Vertical bars are the error bars from the original sources. The shaded range in the Järvinen et al. (2016) data is the range where shape relaxation of 500–1,000 nm particles was observed during cloud chamber expansions. Room temperature data are plotted at 22 °C. Room temperature data of Grayson et al. (2016) are offset for clarity.

The viscosity of humidified SOAs behaved differently from that of pure organics. The sucrose and citric acid viscosity isopleths differ substantially from the α-pinene-derived SOAs observed in this study. The model for these compounds (and their mixtures) is anchored by the transition temperature at 0% RH and by the T_g of pure water at 100% RH via a modified Gordon-Taylor mixing rule and hygroscopicity model (Berkemeier et al., 2014; Koop et al., 2011; Marsh et al., 2018; Rothfuss & Petters, 2017a). The curvature of this isopleth depends on the product of the Gordon-Taylor constant and the hygroscopicity. SOAs from this study have much steeper isopleth that intersect 100% RH near 0 °C and application of the cited Gordon-Taylor model is unable to explain the trend.

Although the dry viscosities are consistent between studies, the viscosities of humidified α-pinene-derived SOAs are not. For example, α-pinene-derived SOA from Zhang et al. (2015), broadly consistent with Renbaum-Wolff et al. (2013), has viscosity ~10^6 Pa·s at 50% RH at room temperature, ~50 °C warmer than the SOA of Järvinen et al. (2016). Results from this study fall between these extremes. Furthermore, the isopleth of Järvinen et al. (2016) has a shallower slope than that of this study. Grayson et al. (2016) demonstrated a systematic decrease of viscosity at room temperature with increasing mass loading during SOA generation. When the Järvinen et al. (2016) measurements are extrapolated toward dry conditions, Figure 4 supports this finding. The observed relaxation for dry α-pinene-derived SOA from this study is consistent with the Grayson et al. (2016) data at similar mass loadings. Differences in these data sets could stem from differences in viscosity measurement or differences in SOA generation and composition. SOA generation techniques are optimized differently for different viscosity measurements. We focus here on potential differences in the properties of the generated SOAs, which are now discussed.

3.1. Diffusion Time Scale

The measurements from Zhang et al. (2015), Järvinen et al. (2016), and this study use coalescence to infer viscosity. Zhang et al. (2015) and Järvinen et al. (2016) use particle agglomerates formed by Brownian coagulation, this study uses synthesized dimers. The sizes and residence times also differ: Zhang et al. (2015) used 126–190 nm particles with coalescence times between 35 and 310 s, Järvinen et al. (2016) used 500–1000 nm particles with 10 min coalescence time. This study uses 100 nm particles with 5 s coalescence time. Water uptake is responsible for reduced viscosity. Therefore, slower water diffusion at cold temperature might be hypothesized to explain the steepness of the viscosity isopleths from this study (Figures 3 and 4). This is unlikely. Rothfuss et al. (2018) measured the time scale for supermicron dry glassy particles to take up water at elevated RH between −10 and 20 °C. Although diffusional limitations were observed, estimated equilibration times scales for submicron particles were <100 ms. However, the Rothfuss et al. (2018) data are limited to hygroscopic single component model compounds such as sucrose. Price et al. (2015) and Lienhard et al. (2015) show data for α-pinene-derived SOA. Their measurements suggest that equilibration time scale for 100 nm particles at 0 °C is at most 1 s (assuming Fickian diffusion), and close to 1 s at −10 °C. Moreover, Lienhard et al. (2015) show that water equilibration with 100 nm α-pinene-derived SOA occurs as fast (or faster) than for sucrose. As demonstrated in Figure 4 the residence time used in this study is suitable to resolve the viscosity transition for sucrose down to −10 °C. Although SOAs differ across studies, we find it unlikely that kinetic limitations explain our steep viscosity isopleth.

3.2. Composition and Solubility

The chemical composition of the SOA from the same precursor under different reaction conditions and between different monoterpene precursors is certainly different. Changes in functional group composition affect hygroscopicity, solubility in water, dry compound viscosity, and indirectly the extent of oligomer formation (Algrim & Ziemann, 2016; Kuwata et al., 2013; M. D. Petters et al., 2016; Rothfuss & Petters, 2017b; Suda et al., 2014). The sensitivity of viscosity and viscosity isopleths to molecular structure, functional group composition, molecular weight, and water content (Rothfuss & Petters, 2017a, 2017b; Shiraiwa et al., 2017) is likely responsible for the diversity of viscosity results for α-pinene-derived SOAs between studies. One possible explanation for the observed steep viscosity isopleth is that the SOA does not absorb water at cold temperatures due to solubility limitations. The effect may also be tied to the SOA generation conditions and may be unique to the method employed here. This study has insufficient data to test these hypotheses. Since the equilibrium water content is critical for understanding the phase diagram, concurrent measurements of water uptake at cold temperature (e.g., Weingartner et al.,

2002) are recommended for future studies. Furthermore, a mechanistic understanding of the range of results for α-pinene-derived SOAs is necessary in order to extrapolate laboratory studies to the phase state of ambient SOA.

4. Summary and Conclusions

The temperature and RH dependence of viscosity was investigated for 100 nm SOA derived from the ozonolysis of five monoterpenes. The observed temperature dependence of viscosity for dry particles was similar to that of citric acid, coal tar pitch, and sorbitol. Glass transition temperatures were obtained by extrapolation of temperature-dependent viscosity to 10^{12} Pa·s. These ranged from −10 to 20 °C (±10 °C). The SOA viscosity (i.e., the temperature at which viscosity was 10^{6} Pa·s) decreased with increasing f_{44} and increased with increasing f_{43}, as determined from mass spectrometry. This suggests that more highly oxidized SOAs were less viscous, likely due to changes in molecular weight. Results from this study are within the large range of literature results for SOA viscosity. Unique to this study, high RH was insufficient to plasticize SOA at cold temperatures. This is unlikely due to diffusional limitations. Prediction of aerosol phase for broader contexts will require an improved understanding of the water uptake at cold temperatures and compositional dependence of SOA viscosity.

Data

Data supporting the conclusions are obtained from the supporting information.

Acknowledgments
This research was funded by the United States Department of Energy, Office of Science grant DE-SC0012043. We thank Patrick Chuang for the HFDMA, Darrel Baumgardner for the RDMA, Timothy Wright for designing and constructing the flow-tube reactor, and Timothy Onasch and John Shilling for discussion of ACSM data interpretation.

References

Abramson, E., Imre, D., Beránek, J., Wilson, J., & Zelenyuk, A. (2013). Experimental determination of chemical diffusion within secondary organic aerosol particles. *Physical Chemistry Chemical Physics*, *15*(8), 2983–2991. https://doi.org/10.1039/C2CP44013J

Aiken, A. C., DeCarlo, P. F., Kroll, J. H., Worsnop, D. R., Huffman, J. A., Docherty, K. S., et al. (2008). O/C and OM/OC ratios of primary, secondary, and ambient organic aerosols with high-resolution time-of-flight aerosol mass spectrometry. *Environmental Science & Technology*, *42*(12), 4478–4485. https://doi.org/10.1021/es703009q

Algrim, L. B., & Ziemann, P. J. (2016). Effect of the keto group on yields and composition of organic aerosol formed from OH radical-initiated reactions of ketones in the presence of NOx. *The Journal of Physical Chemistry. A*, *120*(35), 6978–6989. https://doi.org/10.1021/acs.jpca.6b05839

Bateman, A. P., Bertram, A. K., & Martin, S. T. (2015). Hygroscopic influence on the semisolid-to-liquid transition of secondary organic materials. *The Journal of Physical Chemistry. A*, *119*(19), 4386–4395. https://doi.org/10.1021/jp508521c

Baustian, K. J., Wise, M. E., Jensen, E. J., Schill, G. P., Freedman, M. A., & Tolbert, M. A. (2013). State transformations and ice nucleation in amorphous (semi-)solid organic aerosol. *Atmospheric Chemistry and Physics*, *13*(11), 5615–5628. https://doi.org/10.5194/acp-13-5615-2013

Berkemeier, T., Shiraiwa, M., Pöschl, U., & Koop, T. (2014). Competition between water uptake and ice nucleation by glassy organic aerosol particles. *Atmospheric Chemistry and Physics*, *14*(22), 12513–12531. https://doi.org/10.5194/acp-14-12513-2014

Bilde, M., Svenningsson, B., Mønster, J., & Rosenørn, T. (2003). Even−odd alternation of evaporation rates and vapor pressures of C3−C9 dicarboxylic acid aerosols. *Environmental Science & Technology*, *37*(7), 1371–1378. https://doi.org/10.1021/es0201810

Charnawskas, J. C., Alpert, P. A., Lambe, A. T., Berkemeier, T., O'Brien, R. E., Massoli, P., et al. (2017). Condensed-phase biogenic–anthropogenic interactions with implications for cold cloud formation. *Faraday Discussions*, *200*, 165–194. https://doi.org/10.1039/C7FD00010C

Collier, K. N., & Brooks, S. D. (2016). Role of organic hydrocarbons in atmospheric ice formation via contact freezing. *The Journal of Physical Chemistry. A*, *120*(51), 10,169–10,180. https://doi.org/10.1021/acs.jpca.6b11890

Debenedetti, P. G., & Stillinger, F. H. (2001). Supercooled liquids and the glass transition. *Nature*, *410*(6825), 259–267. https://doi.org/10.1038/35065704

Diamante, L. M., & Lan, T. (2014). Absolute viscosities of vegetable oils at different temperatures and shear rate range of 64.5 to 4835 s^{-1}. *Journal of Food Process*, *2014*(6), 1–6. https://doi.org/10.1155/2014/234583

Fulcher, G. S. (1925). Analysis of recent measurements of the viscosity of glasses. *Journal of the American Ceramic Society*, *8*(6), 339–355. https://doi.org/10.1111/j.1151-2916.1925.tb16731.x

Grayson, J. W., Zhang, Y., Mutzel, A., Renbaum-Wolff, L., Böge, O., Kamal, S., et al. (2016). Effect of varying experimental conditions on the viscosity of α-pinene derived secondary organic material. *Atmospheric Chemistry and Physics*, *16*(10), 6027–6040. https://doi.org/10.5194/acp-16-6027-2016

Gržinić, G., Bartels-Rausch, T., Berkemeier, T., Türler, A., & Ammann, M. (2015). Viscosity controls humidity dependence of N_2O_5 uptake to citric acid aerosol. *Atmospheric Chemistry and Physics*, *15*(23), 13,615–13,625. https://doi.org/10.5194/acp-15-13615-2015

Hinks, M. L., Brady, M. V., Lignell, H., Song, M., Grayson, J. W., Bertram, A. K., et al. (2016). Effect of viscosity on photodegradation rates in complex secondary organic aerosol materials. *Physical Chemistry Chemical Physics*, *18*(13), 8785–8793. https://doi.org/10.1039/C5CP05226B

Hosny, N. A., Fitzgerald, C., Vyšniauskas, A., Athanasiadis, A., Berkemeier, T., Uygur, N., et al. (2016). Direct imaging of changes in aerosol particle viscosity upon hydration and chemical aging. *Chemical Science*, *7*(2), 1357–1367. https://doi.org/10.1039/C5SC02959G

Hritz, A. D., Raymond, T. M., & Dutcher, D. D. (2016). A method for the direct measurement of surface tension of collected atmospherically relevant aerosol particles using atomic force microscopy. *Atmospheric Chemistry and Physics*, *16*(15), 9761–9769. https://doi.org/10.5194/acp-16-9761-2016

Ignatius, K., Kristensen, T. B., Järvinen, E., Nichman, L., Fuchs, C., Gordon, H., et al. (2016). Heterogeneous ice nucleation of viscous secondary organic aerosol produced from ozonolysis of α-pinene. *Atmospheric Chemistry and Physics*, *16*(10), 6495–6509. https://doi.org/10.5194/acp-16-6495-2016

Järvinen, E., Ignatius, K., Nichman, L., Kristensen, T. B., Fuchs, C., Hoyle, C. R., et al. (2016). Observation of viscosity transition in α-pinene secondary organic aerosol. *Atmospheric Chemistry and Physics*, *16*(7), 4423–4438. https://doi.org/10.5194/acp-16-4423-2016

Kidd, C., Perraud, V., Wingen, L. M., & Finlayson-Pitts, B. J. (2014). Integrating phase and composition of secondary organic aerosol from the ozonolysis of α-pinene. *Proceedings of the National Academy of Sciences*, *111*(21), 7552–7557. https://doi.org/10.1073/pnas.1322558111

Koop, T., Bookhold, J., Shiraiwa, M., & Poschl, U. (2011). Glass transition and phase state of organic compounds: Dependency on molecular properties and implications for secondary organic aerosols in the atmosphere. *Physical Chemistry Chemical Physics*, *13*(43), 19238–19255. https://doi.org/10.1039/C1CP22617G

Korosi, G., & Kovats, E. S. (1981). Density and surface tension of 83 organic liquids. *Journal of Chemical & Engineering Data*, *26*(3), 323–332. https://doi.org/10.1021/je00025a032

Kroll, J. H., Donahue, N. M., Jimenez, J. L., Kessler, S. H., Canagaratna, M. R., Wilson, K. R., et al. (2011). Carbon oxidation state as a metric for describing the chemistry of atmospheric organic aerosol. *Nature Chemistry*, *3*(2), 133–139. https://doi.org/10.1038/nchem.948

Kuwata, M., Shao, W., Lebouteiller, R., & Martin, S. T. (2013). Classifying organic materials by oxygen-to-carbon elemental ratio to predict the activation regime of cloud condensation nuclei (CCN). *Atmospheric Chemistry and Physics*, *13*(10), 5309–5324. https://doi.org/10.5194/acp-13-5309-2013

Lambe, A. T., Onasch, T. B., Massoli, P., Croasdale, D. R., Wright, J. P., Ahern, A. T., et al. (2011). Laboratory studies of the chemical composition and cloud condensation nuclei (CCN) activity of secondary organic aerosol (SOA) and oxidized primary organic aerosol (OPOA). *Atmospheric Chemistry and Physics*, *11*(17), 8913–8928. https://doi.org/10.5194/acp-11-8913-2011

Lienhard, D. M., Huisman, A. J., Krieger, U. K., Rudich, Y., Marcolli, C., Luo, B. P., et al. (2015). Viscous organic aerosol particles in the upper troposphere: Diffusivity-controlled water uptake and ice nucleation? *Atmospheric Chemistry and Physics*, *15*(23), 13599–13613. https://doi.org/10.5194/acp-15-13599-2015

Marsh, A., Petters, S. S., Rothfuss, N. E., Rovelli, G., Song, Y. C., Reid, J. P., & Petters, M. D. (2018). Amorphous phase state diagrams and viscosity of ternary aqueous organic/organic and inorganic/organic mixtures. *Physical Chemistry Chemical Physics*, *20*(22), 15086–15097. https://doi.org/10.1039/C8CP00760H

Murray, B. J., Wilson, T. W., Dobbie, S., Cui, Z., Al-Jumur, S. M. R. K., Möhler, O., et al. (2010). Heterogeneous nucleation of ice particles on glassy aerosols under cirrus conditions. *Nature Geoscience*, *3*, 233–237. https://doi.org/10.1038/ngeo817

Ng, N. L., Herndon, S. C., Trimborn, A., Canagaratna, M. R., Croteau, P. L., Onasch, T. B., et al. (2011). An Aerosol Chemical Speciation Monitor (ACSM) for routine monitoring of the composition and mass concentrations of ambient aerosol. *Aerosol Science and Technology*, *45*(7), 780–794. https://doi.org/10.1080/02786826.2011.560211

Pajunoja, A., Lambe, A. T., Hakala, J., Rastak, N., Cummings, M. J., Brogan, J. F., et al. (2015). Adsorptive uptake of water by semisolid secondary organic aerosols. *Geophysical Research Letters*, *42*, 3063–3068. https://doi.org/10.1002/2015GL063142

Pajunoja, A., Malila, J., Hao, L., Joutsensaari, J., Lehtinen, K. E. J., & Virtanen, A. (2014). Estimating the viscosity range of SOA particles based on their coalescence time. *Aerosol Science and Technology*, *48*(2), i–iv. https://doi.org/10.1080/02786826.2013.870325

Petters, M. D., Kreidenweis, S. M., & Ziemann, P. J. (2016). Prediction of cloud condensation nuclei activity for organic compounds using functional group contribution methods. *Geoscientific Model Development*, *9*(1), 111–124. https://doi.org/10.5194/gmd-9-111-2016

Petters, S. S., & Petters, M. D. (2016). Surfactant effect on cloud condensation nuclei for two-component internally mixed aerosols. *Journal of Geophysical Research: Atmospheres*, *121*, 1878–1895. https://doi.org/10.1002/2015JD024090

Price, H. C., Mattsson, J., Zhang, Y., Bertram, A. K., Davies, J. F., Grayson, J. W., et al. (2015). Water diffusion in atmospherically relevant α-pinene secondary organic material. *Chemical Science*, *6*(8), 4876–4883. https://doi.org/10.1039/c5sc00685f

Reid, J. P., Bertram, A. K., Topping, D. O., Laskin, A., Martin, S. T., Petters, M. D., et al. (2018). The viscosity of atmospherically relevant organic particles. *Nature Communications*, *9*(1), 956. https://doi.org/10.1038/s41467-018-03027-z

Renbaum-Wolff, L., Grayson, J. W., Bateman, A. P., Kuwata, M., Sellier, M., Murray, B. J., et al. (2013). Viscosity of α-pinene secondary organic material and implications for particle growth and reactivity. *Proceedings of the National Academy of Sciences*, *110*(20), 8014–8019. https://doi.org/10.1073/pnas.1219548110

Rothfuss, N. E., Marsh, A., Rovelli, G., Petters, M. D., & Reid, J. P. (2018). Condensation kinetics of water on amorphous aerosol particles. *Journal of Physical Chemistry Letters*, *9*(13), 3708–3713. https://doi.org/10.1021/acs.jpclett.8b01365

Rothfuss, N. E., & Petters, M. D. (2016). Coalescence-based assessment of aerosol phase state using dimers prepared through a dual-differential mobility analyzer technique. *Aerosol Science and Technology*, *50*(12), 1294–1305. https://doi.org/10.1080/02786826.2016.1221050

Rothfuss, N. E., & Petters, M. D. (2017a). Characterization of the temperature and humidity-dependent phase diagram of amorphous nanoscale organic aerosols. *Physical Chemistry Chemical Physics*, *19*(9), 6532–6545. https://doi.org/10.1039/C6CP08593H

Rothfuss, N. E., & Petters, M. D. (2017b). Influence of functional groups on the viscosity of organic aerosol. *Environmental Science & Technology*, *51*(1), 271–279. https://doi.org/10.1021/acs.est.6b04478

Saukko, E., Lambe, A. T., Massoli, P., Koop, T., Wright, J. P., Croasdale, D. R., et al. (2012). Humidity-dependent phase state of SOA particles from biogenic and anthropogenic precursors. *Atmospheric Chemistry and Physics*, *12*(16), 7517–7529. https://doi.org/10.5194/acp-12-7517-2012

Shiraiwa, M., Li, Y., Tsimpidi, A. P., Karydis, V. A., Berkemeier, T., Pandis, S. N., et al. (2017). Global distribution of particle phase state in atmospheric secondary organic aerosols. *Nature Communications*, *8*, 15002. https://doi.org/10.1038/ncomms15002

Shrivastava, M., Lou, S., Zelenyuk, A., Easter, R. C., Corley, R. A., Thrall, B. D., et al. (2017). Global long-range transport and lung cancer risk from polycyclic aromatic hydrocarbons shielded by coatings of organic aerosol. *Proceedings of the National Academy of Sciences*, *114*(6), 1246–1251. https://doi.org/10.1073/pnas.1618475114

Slade, J. H., & Knopf, D. A. (2014). Multiphase OH oxidation kinetics of organic aerosol: The role of particle phase state and relative humidity. *Geophysical Research Letters*, *41*, 5297–5306. https://doi.org/10.1002/2014GL060582

Song, M., Liu, P. F., Hanna, S. J., Li, Y. J., Martin, S. T., & Bertram, A. K. (2015). Relative humidity-dependent viscosities of isoprene-derived secondary organic material and atmospheric implications for isoprene-dominant forests. *Atmospheric Chemistry and Physics*, *15*(9), 5145–5159. https://doi.org/10.5194/acp-15-5145-2015

Song, M., Liu, P. F., Hanna, S. J., Zaveri, R. A., Potter, K., You, Y., et al. (2016). Relative humidity-dependent viscosity of secondary organic material from toluene photo-oxidation and possible implications for organic particulate matter over megacities. *Atmospheric Chemistry and Physics*, *16*(14), 8817–8830. https://doi.org/10.5194/acp-16-8817-2016

Suda, S. R., Petters, M. D., Yeh, G. K., Strollo, C., Matsunaga, A., Faulhaber, A., et al. (2014). Influence of functional groups on organic aerosol cloud condensation nucleus activity. *Environmental Science & Technology*, *48*(17), 10182–10190. https://doi.org/10.1021/es502147y

Wagner, R., Höhler, K., Huang, W., Kiselev, A., Möhler, O., Mohr, C., et al. (2017). Heterogeneous ice nucleation of α-pinene SOA particles before and after ice cloud processing. *Journal of Geophysical Research: Atmospheres*, *122*, 4924–4943. https://doi.org/10.1002/2016JD026401

Weingartner, E., Gysel, M., & Baltensperger, U. (2002). Hygroscopicity of aerosol particles at low temperatures. 1. New low-temperature H-TDMA instrument: Setup and first applications. *Environmental Science & Technology*, *36*(1), 55–62. https://doi.org/10.1021/es010054o

Wood, L. J., & Downer, M. (1965). Viscosity/temperature equations for coal tar pitches and refined tars. *Journal of Applied Chemistry*, *15*(9), 431–438. https://doi.org/10.1002/jctb.5010150908

Wright, T. P., Song, C., Sears, S., & Petters, M. D. (2016). Thermodynamic and kinetic behavior of glycerol aerosol. *Aerosol Science and Technology*, *50*(12), 1385–1396. https://doi.org/10.1080/02786826.2016.1245405

Yanniotis, S., Skaltsi, S., & Karaburnioti, S. (2006). Effect of moisture content on the viscosity of honey at different temperatures. *Journal of Food Engineering*, *72*(4), 372–377. https://doi.org/10.1016/j.jfoodeng.2004.12.017

Ye, Q., Robinson, E. S., Ding, X., Ye, P., Sullivan, R. C., & Donahue, N. M. (2016). Mixing of secondary organic aerosols versus relative humidity. *Proceedings of the National Academy of Sciences*, *113*(45), 12649–12654. https://doi.org/10.1073/pnas.1604536113

Yli-Juuti, T., Pajunoja, A., Tikkanen, O. P., Buchholz, A., Faiola, C., Väisänen, O., et al. (2017). Factors controlling the evaporation of secondary organic aerosol from α-pinene ozonolysis. *Geophysical Research Letters*, *44*, 2562–2570. https://doi.org/10.1002/2016GL072364

Zaveri, R. A., Easter, R. C., Shilling, J. E., & Seinfeld, J. H. (2014). Modeling kinetic partitioning of secondary organic aerosol and size distribution dynamics: Representing effects of volatility, phase state, and particle-phase reaction. *Atmospheric Chemistry and Physics*, *14*(10), 5153–5181. https://doi.org/10.5194/acp-14-5153-2014

Zelenyuk, A., Imre, D., Beránek, J., Abramson, E., Wilson, J., & Shrivastava, M. (2012). Synergy between secondary organic aerosols and long-range transport of polycyclic aromatic hydrocarbons. *Environmental Science & Technology*, *46*(22), 12459–12466. https://doi.org/10.1021/es302743z

Zhang, Y., Sanchez, M. S., Douet, C., Wang, Y., Bateman, A. P., Gong, Z., et al. (2015). Changing shapes and implied viscosities of suspended submicron particles. *Atmospheric Chemistry and Physics*, *15*(14), 7819–7829. https://doi.org/10.5194/acp-15-7819-2015

Zobrist, B., Marcolli, C., Pedernera, D. A., & Koop, T. (2008). Do atmospheric aerosols form glasses? *Atmospheric Chemistry and Physics*, *8*(17), 5221–5244. https://doi.org/10.5194/acp-8-5221-2008